

## Composition and Evolution of the Mantle and Core

Seismology and solid state physics place strong constraints on the constitution of the earth's interior.

Don L. Anderson, Charles Sammis, Tom Jordan

In 1952 Birch published a remarkable paper on the elasticity and constitution of the earth's interior (*1*). This pioneering work laid the foundation for most subsequent research in this field. Since then, a considerable body of seismic, ultrasonic, shock-wave, static compression, and petrologic data has been accumulated. The use of surface waves and large seismic arrays has led to refinements in the velocity structure of the earth's interior, particularly in the important transition region of the upper mantle. Free oscillations have made a direct determination of density possible and have supplied a new parameter, the seismic anelasticity of the various regions of the mantle. Shock-wave data are now available for a number of metals, rocks, and minerals to pressures of the order of a megabar and more. Ultrasonic measurements have been made on a variety of important rocks and minerals and, in many cases, include the effect of temperature and pressure. High-pressure techniques in experimental petrology have provided information on the crystal structures and densities of high-pressure phases of mantle minerals and have defined the stability fields and melting relations of many important geophysical systems. The use of dia-

Dr. Anderson is professor of geophysics and director of the Seismological Laboratory, Division of Geological Sciences, California Institute of Technology, Pasadena. His coauthors are also affiliated with the Seismological Laboratory.

mond anvils and x-rays has considerably improved and extended the pressure range of static compression experiments.

This article makes use of many of these data to interpret the properties of the various regions of the earth's interior, but it is far from being a complete synthesis of all available information.

### Structure of the Mantle and Core

The basic divisions of the earth—that is, crust, mantle, liquid outer core, and solid inner core—have been known for some time. Considerable refinement has been possible in the last 10 years with the advent of large aperture seismic arrays, the worldwide network of standardized seismic stations, large underground explosions, and the use of long-period surface waves. The compressional velocity and the shear velocity are now fairly well determined throughout the earth from body-wave studies. The periods of the earth's free oscillations, which can be measured after large earthquakes, provide data relevant to the distribution of density in the earth, although not with the resolving power available from body waves for the seismic velocities.

In Fig. 1, the compressional velocity  $V_p$ , the shear velocity  $V_s$ , and density  $\rho$  are shown as functions of radius in

the earth. The model shown (model 435002) is consistent with the earth's mass, moment of inertia, periods of free oscillation, and travel times of body waves. The inversion of seismic data to models of the earth's interior is a subject of much current interest. The mathematical and physical arguments that lead to the present model will not be discussed here, but it represents an optimum solution to the linear inverse geophysical problem. Model 435002 satisfies free oscillation, surface-wave dispersion, and body-wave travel-time data to within a root-mean-square error of 0.23 percent.

The major regions of the earth's interior may be summarized as follows:

1) The upper mantle consists of a thin (0 to 50 kilometers thick) high-velocity layer which, together with the crust, constitutes the lithosphere, the strong outer layer of the earth which overlies the low-velocity zone, a partly molten layer of the order of 100 kilometers in thickness (the asthenosphere). Most of the world's earthquake activity occurs in the lithosphere, which reacts to stresses as a brittle solid. From a depth of about 150 to 400 kilometers the mantle is relatively homogeneous; its properties can be explained by self-compression in the presence of a moderate temperature gradient.

The important minerals of the upper mantle are olivine, pyroxene, and garnet in their familiar low-pressure phases. Spinel and amphibole are the dominant accessory minerals near the top of the upper mantle.

2) The transition region (at a depth of 400 to 800 kilometers) is characterized by several abrupt increases in velocity, which can be attributed to pressure-induced changes in crystal structure. These changes ultimately result in a mineral assemblage that is some 20 percent denser than the corresponding assemblage in the upper mantle. Laboratory measurements at high pressures have shown that olivine, the major component of the mantle, transforms to a spinel type of structure at pressures corresponding to a depth of about 400 kilometers. This structure is

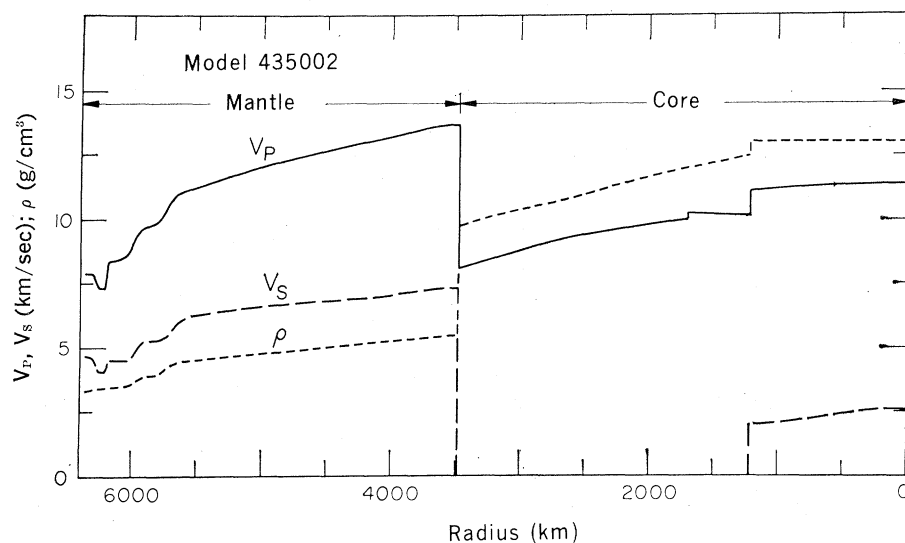


Fig. 1. Compressional velocity  $V_p$ , shear velocity  $V_s$ , and density  $\rho$  as a function of radius in the earth, determined by the inversion of mass, moment of inertia, body-wave travel-time, and free oscillation data (3, 47).

7½ to 10 percent denser than the low-pressure phase. The major discontinuities in the mantle occur at depths of 400 to 600 kilometers. Below some 600 kilometers much of the silicon is in six-fold coordination with oxygen. Earthquakes do not occur below 700 kilometers, a fact probably related to the major change of coordination that occurs in mantle minerals near this depth.

3) The lower mantle is relatively homogeneous; that is, the velocities and density increase monotonically owing to self-compression, with no major solid-solid phase changes. There are minor discontinuities in the lower mantle, however, which account for approximately 17 percent of the total increase of velocity in this region. The density gradient in the lower mantle, inferred from free oscillation data, is less than that inferred from the assumption that this region is homogeneous and adiabatic.

4) The lower mantle transition zone, just above the core, is a region

where the velocities may be relatively constant, but the interpretation is complicated by diffraction effects at the mantle-core boundary.

5) The density and compressional velocity change abruptly at the mantle-core boundary, and no shear waves are able to penetrate this interface. Thus, the outer core is liquid; it has the properties of molten iron mixed with sulfur or silicon. Motions in the fluid outer core are probably responsible for the earth's magnetic field, although there is some evidence that these motions have not completely homogenized this region of the earth. The outer core may be chemically zoned.

6) The inner core is believed to be solid on the basis of indirect evidence and free oscillation data, but the low shear velocity, relative to the compressional velocity, suggests that it is near the melting point or is partly molten. The density appears to be nearly continuous across the outer core-inner core boundary, but the compressional

velocity increases substantially. The boundary between the outer and inner core may be a liquid-solid phase change boundary or a compositional boundary. The density of the inner core is approximately 13 grams per cubic centimeter.

In this article we will infer the chemical composition of the various regions of the earth on the basis of the seismic data in conjunction with finite strain theory and on the basis of laboratory measurements of shock-wave and ultrasonic properties.

### Mineralogy of the Upper Mantle

Ultrasonic data are now available for many of the minerals that are thought to occur in the upper mantle (2). Temperature and pressure derivatives are available for olivine, garnet, and spinel but not for amphibole, feldspars, or pyroxene. The interpretation of the seismic data is complicated by the lateral variability of the velocity in the upper 200 kilometers of the mantle. Below 200-kilometer depth the various solutions tend to be fairly consistent, although even at these depths there is some evidence for lateral heterogeneity.

For illustrative purposes we will take recent seismic solutions (3), which give, at 200 kilometers,  $V_p = 8.30$  kilometers per second,  $V_s = 4.64$  km/sec, and  $\rho = 3.5$  g/cm<sup>3</sup>. Hales and Roberts and Helmberger and Wiggins (4) give, for this depth,  $V_p = 8.65$  km/sec and  $V_s = 4.60$  km/sec. In order to compare these values with ultrasonic data, they must be corrected to room temperature and pressure. We will assume that the temperature and pressure at 200 kilometers are 1200°C and 67 kilobars, respectively, and will adopt the following values for the derivatives (2):

$$(\partial V_p / \partial P)_T = 10 \times 10^{-3} \text{ km/sec} \cdot \text{kb}$$

$$(\partial V_s / \partial P)_T = 3 \times 10^{-3} \text{ km/sec} \cdot \text{kb}$$

$$(\partial V_p / \partial T)_P = -4 \times 10^{-4} \text{ km/sec} \cdot ^\circ\text{C}$$

$$(\partial V_s / \partial T)_P = -3 \times 10^{-4} \text{ km/sec} \cdot ^\circ\text{C}$$

$$\alpha = -\frac{1}{\rho} \frac{\partial \rho}{\partial T} = 20 \times 10^{-6} / ^\circ\text{C}$$

where  $T$  is temperature,  $\rho$  is pressure, and  $\alpha$  is the volume coefficient of thermal expansion. With these parameters the properties of the mantle at standard conditions are as given in Table 1. Also given in this table are velocities and densities of olivine, py-

Table 1. Velocities and densities of the mantle, of mantle minerals (2), and of various mixes. The olivine is 93 mole percent forsterite; the pyroxene is 85 mole percent enstatite. The garnet is of almandite-pyrope composition (2). Mix 1 is pyrolite, with the following composition (in weight percent): olivine, 56; pyroxene, 35; and garnet, 9 (42). Mix 2 has the following composition (in weight percent): olivine, 40; pyroxene, 50; and garnet, 10. STP, standard temperature and pressure.

Property	Mantle at 200 km		Olivine	Pyroxene	Garnet	Mix 1	Mix 2
	Ambient	STP					
$V_p$ (km/sec)	8.30–8.65	8.11–8.46	8.42	7.85	8.53	8.22	8.14
$V_s$ (km/sec)	4.52–4.60	4.80–4.88	4.89	4.76	4.76	4.83	4.81
$\rho$ (g/cm <sup>3</sup> )	3.50	3.42	3.31	3.34	4.16	3.38	3.39

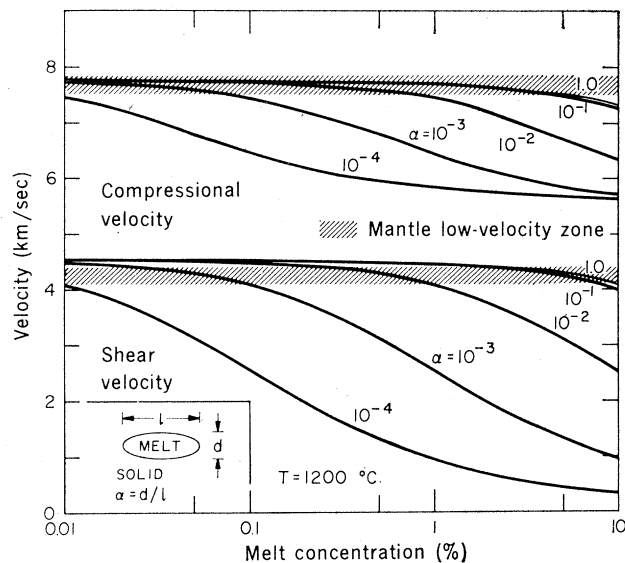
roxene, and garnet (all natural single crystals) and computed properties for two mixtures of these minerals. The present uncertainty in seismic velocities in the upper mantle, below the low-velocity zone, will allow mineralogies ranging (in percent by weight) from 100 percent olivine to 40 percent olivine, 50 percent pyroxene, and 10 percent garnet. On the basis of ultrasonic measurements of ultrabasic rocks, it was concluded earlier (5) that the composition of the mantle near 200-kilometer depth could be explained with a mineralogy of 45 to 75 percent olivine, 20 to 50 percent pyroxene, and up to about 15 percent garnet. These bounds will be considerably reduced when the discrepancy in the seismic data is resolved, but it is encouraging that there is no basic disagreement between the seismic, ultrasonic, and petrologic data.

### Low-Velocity Zone

The interpretation of seismic velocities in terms of composition is complicated by the presence of a region in the upper mantle of abnormally low velocities and high seismic attenuation. The velocities in the low-velocity zone are too low to be explained by any reasonable mineralogy or temperature gradient (6), and, in addition, the boundaries of this zone are apparently quite sharp (7). By combining ultrasonic, petrologic, heat flow, and melting relations, it was concluded (6) that this zone could best be explained by partial melting, or dehydration, of a mineral assemblage containing a small amount of water.

Walsh (8) has used the theory of Eshelby (9) to derive equations for the elastic-wave velocities in a two-phase material composed of a solid isotropic matrix with randomly oriented, penny-shaped melt zones. The velocities are a function of the elastic properties of the two phases, the melt concentration, and the aspect ratio of the melt zones. Birch (10) calculated the velocities of an olivine matrix containing spherical inclusions of basaltic glass with zero rigidity as an approximation to partly molten material. He concluded that the low-velocity zone could be explained by a melt concentration of approximately 6 percent. Penny-shaped pores more nearly approximate the situation for grain boundary melting and adequately ac-

Fig. 2. Compressional and shear velocity as a function of melt concentration and melt zone aspect ratio for a solid olivine matrix containing ellipsoidal pockets of basalt melt. The stippled regions show the range of velocities in the low-velocity zone.



count for the only pertinent experimental data (11).

The Eshelby-Walsh theory and the parameters of Birch (10) were used to plot the compressional and shear velocities as a function of melt concentration in Fig. 2. The upper curves are for  $\alpha = 1$ , which corresponds to spherical melt zones, the case that Birch considered; here,  $\alpha$  is the aspect ratio of the inclusions. Because of the importance of the geometry, the velocities in the low-velocity zone cannot be unambiguously interpreted in terms of melt content. If the aspect ratio  $\alpha$  is as small as  $10^{-2}$ , a melt content of only 1 percent is required to decrease the velocities to the lowest values measured in the low-velocity zone. Since the components that melt at low temperatures will probably be concentrated at grain boundaries, this is not an unreasonable aspect ratio.

### Lower Mantle: Finite Strain Theory and Seismic Velocities

Since the high-pressure phases of the lower mantle are not available for direct study, a different approach must be taken to infer the composition and crystal structure of this region of the mantle. We will utilize finite strain theory to infer the density and velocities of the lower mantle at standard conditions.

Birch (12), in the first attempt to calculate the variation of seismic velocities due to self-compression of a homogeneous spherical shell in a gravitational field, concluded that the density and velocities in the upper mantle

could be explained adequately by finite strain theory but that the gradient of velocities in the lower mantle required a gradual change in composition.

Birch derived the following equations for the compression velocity  $V_p$  and shear velocity  $V_s$ , as functions of the hydrostatic strain  $\epsilon$ , the Lamé parameters  $\lambda$  and  $\mu$ , and the density  $\rho$ :

$$\rho V_p^2 = (1 - 2\epsilon)^{5/2} [\lambda + 2\mu - \epsilon(11\lambda + 10\mu)] \quad (1)$$

and

$$\rho V_s^2 = (1 - 2\epsilon)^{5/2} [\mu - \epsilon(3\lambda + 4\mu)] \quad (2)$$

These equations were derived by truncating the expansion of the strain energy function at the second-order term before differentiating with respect to the appropriate strain. The bracketed expressions in Eqs. 1 and 2 are, therefore, incomplete to first order in strain since the differentiation brings in the coefficients of the higher-order terms in the strain energy expansion.

The complete first-order Eulerian expressions for velocity are (13)

$$\rho V_p^2 = (1 - 2\epsilon)^{5/2} \left[ \lambda + 2\mu - \epsilon(11\lambda + 10\mu - 18l - 4m) \right] \quad (3)$$

and

$$\rho V_s^2 = (1 - 2\epsilon)^{5/2} \left[ \mu - \epsilon(3\lambda + 4\mu + \frac{3}{2}m + \frac{n}{2}) \right] \quad (4)$$

where  $l$ ,  $m$ , and  $n$  are the third-order coefficients in the expansion of the elastic energy density in terms of the

strain invariants, as given by Birch (12).

For hydrostatic compression it is not necessary to know the individual values of  $l$ ,  $m$ , and  $n$  but only the combinations

$$\zeta = 18l + 4m \quad (5)$$

and

$$\eta = \frac{1}{2}(3m + n) \quad (6)$$

When samples are available, these parameters can be determined from hydrostatic ultrasonic measurements and can be expressed in terms of the pressure derivatives of the two seismic velocities

$$\frac{1}{V_p} \frac{\partial V_p}{\partial P} = \frac{1}{6K} \frac{13\lambda + 14\mu - \zeta}{\lambda + 2\mu} \quad (7)$$

$$\frac{1}{V_s} \frac{\partial V_s}{\partial P} = \frac{1}{6K} \frac{3\lambda + 6\mu + \eta}{\mu} \quad (8)$$

evaluated at  $P=0$ . In all of the above expressions,  $K$ ,  $\lambda$ , and  $\mu$  refer to the zero-pressure bulk modulus and Lamé parameters. Similar expressions have been derived by using a Lagrangian coordinate system (14).

The elastic constants and velocity derivatives have been determined for a number of oxides and silicates by ultrasonic techniques. Hence, it is possible, from Eqs. 7 and 8, to calculate the third-order elastic constants  $\zeta$  and  $\eta$ . These parameters are listed in Table 2 for 12 compounds. Note that these higher-order parameters are of the same order as the ordinary elastic constants  $K_s$  and  $\mu$ .

Birch (12) attempted to fit Eqs. 1 and 2 to the seismic velocities in the lower mantle but was unable, by any adjustment of parameters, to satisfy the velocity gradients. He therefore speculated that the lower mantle was inhomogeneous and had a varying composition with depth.

However, the complete first-order expressions (Eqs. 3 and 4) have enough additional flexibility to satisfy the seismic data for the lower mantle very well, as is shown by the middle curves in Fig. 3. The density model used in this calculation is an Adams-Williamson solution; that is, it is determined directly from the seismic velocities on the assumption of homogeneity and adiabaticity. The density gradient in the lower mantle, obtained from the inversion of free oscillation data, is less than that obtained by classical techniques, and the nature of the finite strain fits to this region of the mantle indicates that it departs slightly from the homogeneous-adiabatic assumption. The allowable superadiabatic temperature gradient is less than  $0.3^\circ$  per kilometer. The required second-order parameters are quite reasonable when compared with the ultrasonic measurements of silicates and oxides given in Table 2. Note that it is possible, within the framework of even first-order finite strain theory and with reasonable parameters, to have the shear velocity decrease with pressure even though the corresponding compressional velocities are increasing with pressure. This

is in agreement with lattice calculations of the properties of certain crystal structures (15, 16). Certain materials (for instance,  $\text{SiO}_2$ ,  $\text{Ni}_2\text{FeO}_4$ ,  $\text{ZnO}$ , and  $\text{MgAl}_2\text{O}_4$ ) have shear velocities that decrease with pressure or increase very slowly. Anderson and Liebermann (15) discuss the implications of a negative shear velocity pressure derivative with regard to crystal instability. It is noteworthy that the spinel structure (that is,  $\text{MgO} \cdot 2.6 \text{Al}_2\text{O}_3$  and  $\text{Ni}_2\text{FeO}_4$ ) has very small or negative shear velocity pressure derivatives (Table 2) and that certain seismic solutions for the spinel region of the mantle, between 400 and 600 kilometers (3) show negative shear velocity gradients. The effect of a temperature gradient would accentuate this tendency.

The equation of state consistent with Eqs. 3 and 4 is

$$P = -3K\epsilon(1 - 2\epsilon)^{5/2}(1 + 2\epsilon\xi) \quad (9)$$

where

$$\xi = \frac{3\zeta + 4n}{12K}$$

is the parameter introduced by Birch (1). By simultaneously fitting Eqs. 3, 4, and 9 to seismic  $V_p$ ,  $V_s$ , and profiles, it is possible to solve for the zero-pressure parameters  $V_{p0}$ ,  $V_{s0}$ , and  $\rho_0$  and the second-order finite strain parameters  $\xi$  and  $\eta$  for the various regions of the mantle. Excellent fits can be obtained for most earth models, as is shown in Table 3, which contains

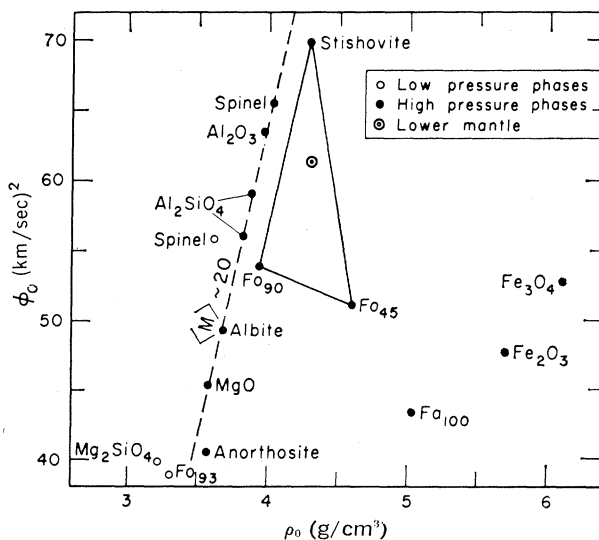
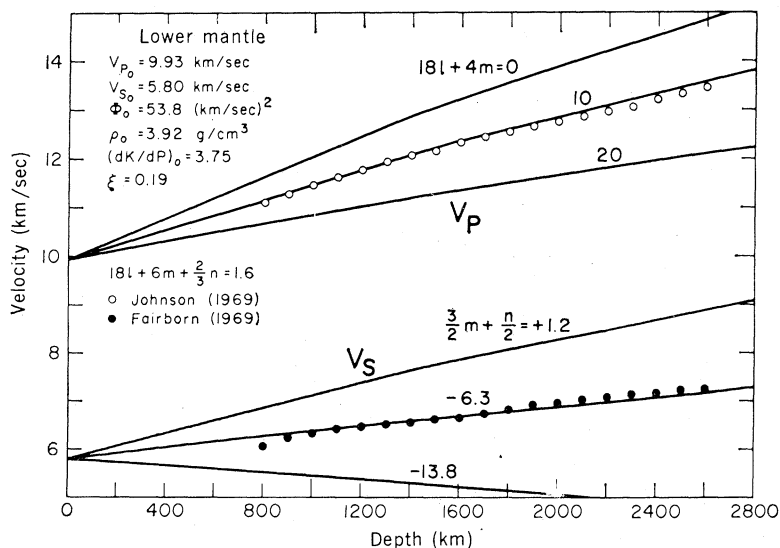


Fig. 3 (left). Compressional velocity ( $V_p$ ) and shear velocity ( $V_s$ ) as a function of depth for various values of the parameters  $18l + 4m$  and  $(3m + n)/2$ . For these calculations  $18l + 6m + 2n/3$  is constrained to  $+1.6$ , a value consistent with the variation of density with depth (18). The earth models are tabulated in (3) and (48). Fig. 4 (right). A plot of  $\Phi_0$  versus  $\rho_0$  from shock-wave experiments for various rocks and minerals (5) and one solution for the lower mantle (18). The seismic parameter  $\Phi_0 = K_0/\rho_0 = V_{p0}^2 - (4/3)V_{s0}^2$ . Iron-free minerals have a mean atomic weight  $\langle M \rangle$  near 20. Iron-bearing minerals fall to the right of the dashed line.

fits to several seismic solutions for the lower mantle. The first two models are from Birch (17). The rest of the models are the results of inverting free oscillation, surface-wave, and travel-time data (18). If the lower mantle has an adiabatic temperature gradient, the parameters given in Table 3 are appropriate for zero pressure and some high temperature [ $\sim 1600^\circ\text{C}$  (18, 19)] which represents the lower mantle adiabatic gradient extrapolated to  $P = 0$ .

The method outlined above [see also (13)] provides a framework for using laboratory data on elastic constants to calculate the seismic velocities at high pressure in a manner consistent with conventional methods of extrapolating density. Density values computed at high pressures from ultrasonic data with the Murnaghan or Birch-Murnaghan finite strain equations of state compare favorably with those found by static or shock-wave compression experiments. This gives some assurance that the ultrasonic data can be reliably extrapolated at least to moderate compressions with finite strain theory.

Similarly, a framework has been established to extrapolate mantle seismic data to zero pressure. In this application the finite strain formulation for the velocities is unique in that no assumption of composition is necessary. More sophisticated finite strain formulations (20) and lattice calculations (15) are all cast in terms of the elastic constants and thus require the specification of composition and crystal structure before they may be applied. Previous discussions of the composition of the deep mantle have been based on  $\rho_0$  and  $\Phi_0 = V_{p0}^2 - (4/3)V_{s0}^2$ . The usefulness of the additional parameter now available is limited by the availability of ultrasonic data on appropriate crystal structures. The shear velocity and its pressure derivatives appear to be more sensitive to coordination effects and details of the crystal structure and may prove to be decisive in understanding the crystal structure of the lower mantle.

With use of the modified form of the seismic equation of state (21)

$$\rho_0 / \langle M \rangle = 0.0492 \Phi_0^{2/3}$$

where

$$\Phi_0 = V_{p0}^2 - (4/3)V_{s0}^2$$

the mean atomic weight  $\langle M \rangle$  for the lower mantle models of Table 3, corrected to room temperature, ranges from 21.6 to 22.6. With a different set of earth models, values from 21.2 to

22.2 have been found (18). The values for  $\zeta$  and  $\eta$  are comparable to those for such close-packed oxides as  $\text{Al}_2\text{O}_3$ ,  $\text{Fe}_2\text{O}_3$ ,  $\text{MgAl}_2\text{O}_4$ , and  $\text{NiFe}_2\text{O}_4$  but are significantly different from olivine, garnet,  $\text{MgO}$ , and  $\text{TiO}_2$ . The normalized velocity derivatives may be more meaningful parameters to compare with the ultrasonic data. For the lower mantle  $d \ln V_p / dP$  is about 0.4 to 0.6 and  $d \ln V_s / dP$  is about 0.2 to 0.3. The closest matches are  $\text{Al}_2\text{O}_3$  and  $\text{Fe}_2\text{O}_3$ ; both have  $\text{M}_2\text{O}_3$  stoichiometry and corundum structure. Rutile, garnet, spinels, and olivines have quite different values. Whether this is evidence for a predominantly  $\text{M}_2\text{O}_3$  stoichiometry such as pyroxene or for a crystal symmetry involving hexagonal close pack of oxygen ions (or both) remains to be seen. Ultimately, the second-order parameters  $\zeta$  and  $\eta$  may provide useful information pertinent to the crystal structure of the lower mantle.

## Lower Mantle: Composition

Figure 4 illustrates how shock-wave data, seismic data, finite strain theory, and the seismic equation of state can be used in discussions of the composition of the deep mantle. The dark circles are shock-wave data of McQueen *et al.* reduced by the method of Anderson and Kanamori (22). The raw shock-wave data are reduced to adiabats which are constrained, in the absence of ultrasonic data, to satisfy the seismic equation of state at zero pressure and to satisfy the Birch-Murnaghan equation of state at high pressure. This yields values for  $\rho_0$  and  $\Phi_0 = (\partial P / \partial \rho)_0$  for phases that are not available for measurement at standard conditions. The lower mantle point is a temperature-corrected Birch-Murnaghan extrapolation of mantle  $\rho$  and  $\Phi$  data (18), obtained from inversion of free oscillation data (model 200204). The

Table 2. Velocity derivatives and finite strain parameters for oxides. [Values for forsterite and olivine are from (43); for trevorite, from (44); and for rutile, from (45). All other values are from (2).]

Material	$\frac{1}{V_p} \frac{dV_p}{dP}$ ( $10^{-12}$ ) cm <sup>2</sup> /dyne	$\frac{1}{V_s} \frac{dV_s}{dP}$ ( $10^{-12}$ ) cm <sup>2</sup> /dyne	$K_s$ ( $10^{12}$ ) dyne/cm <sup>2</sup>	$\mu$ ( $10^{12}$ ) dyne/cm <sup>2</sup>	$\zeta$ ( $10^{12}$ ) dyne/cm <sup>2</sup>	$-\eta$ ( $10^{12}$ ) dyne/cm <sup>2</sup>
Forsterite ( $\text{Mg}_2\text{SiO}_4$ )	1.249	.714	1.286	.811	-1.8	2.6
Olivine ( $\text{Fo}_{.88}\text{Fa}_{.12}$ )	1.211	.737	1.294	.791	-1.0	2.5
Periclase ( $\text{MgO}$ )	.862	.665	1.622	1.308	-0.2	1.6
Lime* ( $\text{CaO}$ )	1.309	.603	1.059	.761	0.6	3.3
Bromelite* ( $\text{BeO}$ )	.538	.0449	2.201	1.618	6.3	12.1
Zincite* ( $\text{ZnO}$ )	.613	-1.138	1.394	.442	10.3	10.2
Corundum ( $\text{Al}_2\text{O}_3$ )	.478	.347	2.521	1.613	7.6	5.5
Hematite* ( $\text{Fe}_2\text{O}_3$ )	.591	.151	2.066	.910	7.7	8.1
Spinel ( $\text{MgO} \cdot 2.6 \text{Al}_2\text{O}_3$ )	.494	.0762	2.020	1.153	11.1	9.6
Trevorite* ( $\text{NiFe}_2\text{O}_4$ )	.610	-.0082	1.823	.713	9.0	8.4
Garnet (Al-Py)	.919	.456	1.770	.943	-1.5	4.5
Rutile ( $\text{TiO}_2$ )	.825	.101	2.155	1.124	-3.9	9.3
Lower mantle†			1.94	1.30	6.9	.65
			2.19	1.43	15.9	7.9

\* Polycrystalline.

† Range of values from Table 3.

Table 3. Finite strain parameters and fits for various lower mantle models. RMS, root mean square.

Model	$\rho_0$ (g/cm <sup>3</sup> )	$V_{p0}$ (km/sec)	$V_{s0}$ (km/sec)	$(10^{12})$ dyne/cm <sup>2</sup>	$-\eta$ ( $10^{12}$ ) dyne/cm <sup>2</sup>	RMS Error (%) in		
						$\rho$	$V_P$	$V_S$
<i>Birch models</i>								
Birch I	3.91	9.80	5.78	8.35	5.80	0.64	0.48	0.26
Birch II	3.96	9.70	5.77	6.57	5.59	0.12	0.57	0.28
<i>Free oscillation models</i>								
200202	4.10	9.89	5.84	9.80	6.92	0.31	0.66	0.27
201104	4.06	10.03	5.91	12.76	7.49	0.37	1.00	0.39
300711	3.96	10.04	6.01	14.30	7.79	0.45	1.71	0.67
301703	3.94	10.00	6.00	13.47	7.64	0.45	1.60	0.67
304702	3.86	10.11	6.06	15.92	7.89	0.47	1.93	0.77
402203	3.93	9.77	5.87	6.94	6.52	0.13	0.41	1.58
402803	3.93	9.85	5.93	8.44	6.95	0.16	0.39	1.48
402813	3.90	9.95	6.02	10.80	7.48	0.22	0.55	1.20

mantle point falls in the field defined by  $\text{Fo}_{90}$ , that is,  $[(\text{Mg}_{0.90}\text{Fe}_{0.10})_2\text{SiO}_4]$ ;  $\text{Fo}_{45}$ , that is,  $[(\text{Mg}_{0.45}\text{Fe}_{0.55})_2\text{SiO}_4]$ ; and  $\text{SiO}_2$  (stishovite). The inferred composition of the lower mantle for this model is  $0.32 \text{ MgO} + 0.18 \text{ FeO} + 0.50 \text{ SiO}_2$  (molar) or  $(\text{Mg}_{0.64}\text{Fe}_{0.36})\text{SiO}_3$ . A slightly different technique (5) gave  $0.38 + 0.16 \text{ FeO} + 0.46 \text{ SiO}_2$  (molar) for the same model and  $0.49 \text{ MgO} + 0.12 \text{ FeO} + 0.39 \text{ SiO}_2$  (molar) for the second Birch model. These compositions imply pyroxene contents of 80 and 43 percent, respectively. Other free oscillation models require less  $\text{SiO}_2$  in the lower mantle, but all models fall well above the high-pressure olivine line (that is, the base of the triangular region) and require considerably more FeO than is typical of upper mantle petrologies; this does not mean, however, that free FeO is necessary in the lower mantle. A conclusive study of the composition of the lower mantle will require shock-wave data on garnets, relatively iron-rich pyroxenes, and such natural rocks as eclogites and pyroxenites.

Birch (23) demonstrated a relation-

ship between density, compressional velocity, and mean atomic weight for rocks and minerals. He speculated that there was a unique relation between density and compressional velocity at constant mean atomic weight, regardless of whether the density change was due to crystal structure effects, pressure, or temperature. In lieu of a theory that provided an estimate of the change of velocity with pressure, he proposed that the density in the earth could be found from the compressional velocity by applying the systematics found at low pressure. This conjecture can now be tested with available ultrasonic data.

Figures 5 and 6 are Birch diagrams showing the relation between velocity and density with mean atomic weight as a parameter. For compressional velocity, the linear relation between  $V_p$  and  $\rho$  for minerals of the same mean atomic weight is well substantiated. In addition, one can draw isostructural lines—for example, for the spinels and olivines.

The light dashed lines in Fig. 5 are  $V_p$ - $\rho$  trajectories calculated from the complete first-order finite strain expres-

sions (Eqs. 3 and 4) and the ultrasonic data in Table 2. In most cases the trend of the pressure trajectories is similar to the slope of the lines of constant mean atomic weight. The effect of a  $1000^\circ\text{K}$  rise in temperature is also shown.

An extrapolated value for the lower mantle is also shown in Fig. 5. The hatched region is an estimate of the room temperature value of  $\rho_0$  and  $V_{p0}$  to provide direct comparison with the values for the oxides and silicates. The mean atomic weight consistent with the temperature-corrected value for the lower mantle is 21.0 to 21.7, which can be compared with the earlier estimates of 22.5 (23), 22.8 to 22.9 (24), and 21.0 to 23.7 (18). Previous estimates of the zero-pressure density of the lower mantle are  $3.93 \pm 0.03$  (23),  $4.15 \pm 0.05$  (19), and  $4.0 \pm 0.1$  (18). The compressional velocity lies well above the spinel line, as might be expected for the closer-packed phases of the lower mantle.

The  $V_s$ - $\rho$  systematics (Fig. 6) are not so regular as the  $V_p$ - $\rho$  systematics, and the  $\langle M \rangle \sim 20$  line is schematic.

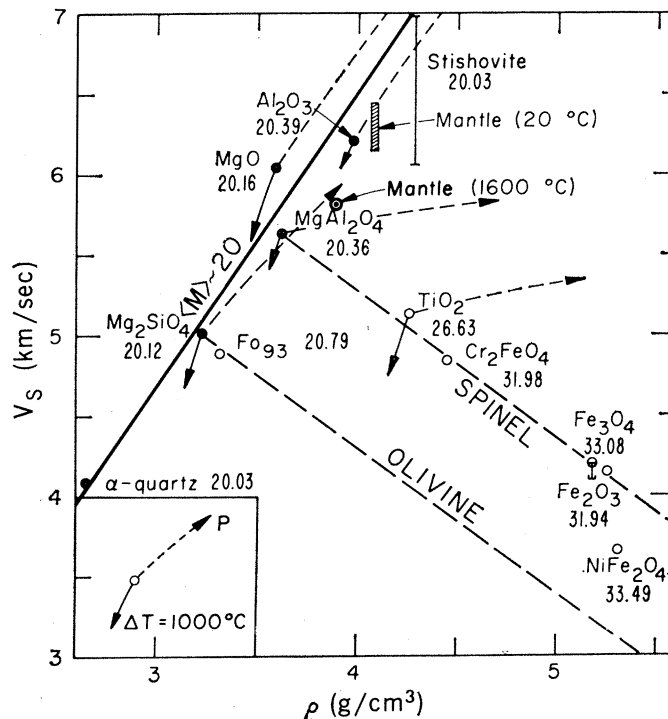
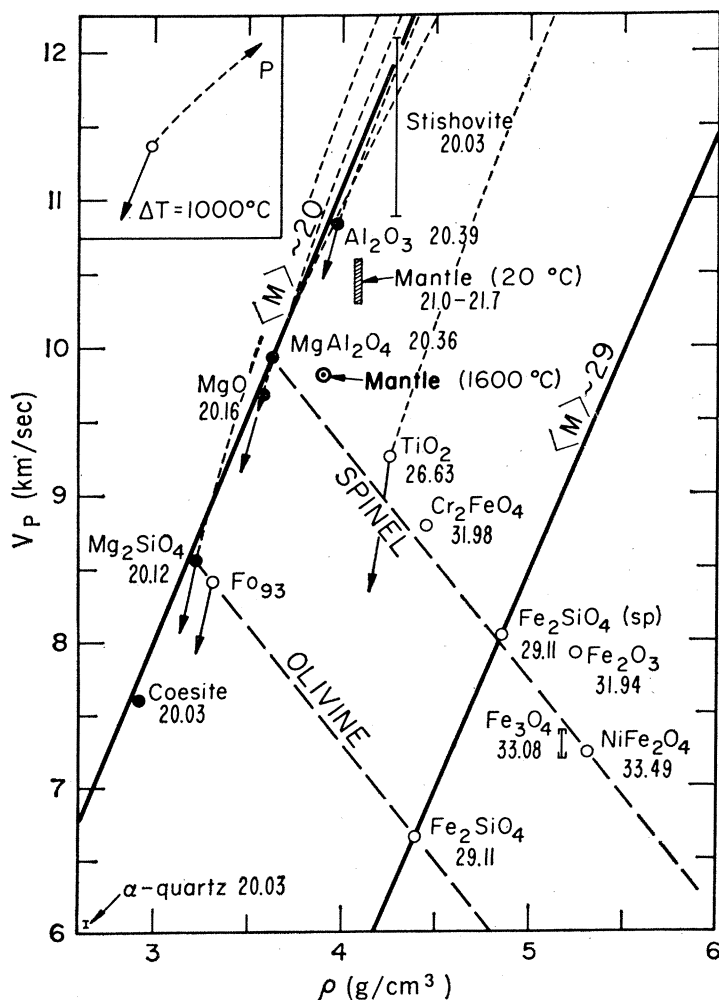


Fig. 5 (left). Compressional velocity versus density for various oxides and silicates (2, 44, 45, 48). The dark circles are minerals with mean atomic weight near 20. The light dashed lines are pressure trajectories calculated from finite strain theory and the parameters of Table 2. The solid lines with arrows show the effect of  $1000^\circ\text{C}$  rise in temperature. Fig. 6 (right). Shear velocity versus density for various oxides and silicates. The effect of pressure is shown by the light dashed lines; of temperature, by the solid lines with arrows.

The dark circles are oxides with mean atomic weight near 20; the scatter indicates that structural effects may be more important for shear waves than for compressional waves.

The spinel and olivine lines are also schematic. The pressure trajectories show a much greater variability than the corresponding curves for the compressional velocity. This is again attributed to the crystal structure effects, which apparently are more important for the pressure derivatives of the shear velocity. Some materials (for instance, rutile and spinel) have very low-pressure derivatives of shear velocity or have negative derivatives (for instance, ZnO, quartz, NiFe<sub>2</sub>O<sub>4</sub>). Between depths in the mantle of about 400 to 600 kilometers, olivine is in the spinel structure, and the shear velocity gradient in this region is constant or slightly negative (3).

An extrapolated value for the lower mantle is also shown in Fig. 6. Because of the scatter and the lack of a simple relation between density,  $V_{ss}$ , and mean atomic weight, the only conclusion is that the mean atomic weight of the lower mantle is consistent with that found from the compressional velocity. When data on more close-packed oxides are available, it should be possible to speculate on the crystal structure of the lower mantle from these diagrams. For the moment, all that can be said is that the density and velocity are consistent with a denser ionic packing than occurs in such close-packed oxides as MgO, MgAl<sub>2</sub>O<sub>4</sub>, and garnets. In these compounds the packing ratio, defined as the fraction of the cell volume that is occupied by ions, ranges from 0.63 to 0.66. The lower mantle has a packing fraction of 0.72, which is close to that of Al<sub>2</sub>O<sub>3</sub>. For comparison, stishovite, the high-pressure form of SiO<sub>2</sub> with the Si ions in sixfold coordination with the oxygen ions, has a packing fraction of 0.84. High-pressure structures of magnesium (aluminum silicates with Si in sixfold coordination) would have packing fractions of approximately 0.70 (forsterite stoichiometry), 0.73 (pyrope stoichiometry), and 0.74 (enstatite stoichiometry).

## Core

The molten outer core is generally considered to be an iron-nickel melt containing a lighter alloying element or elements. The zero-pressure density of molten iron at 1540°C is 7.02

g/cm<sup>3</sup>. At room temperature the density would be 7.13 to 7.23 g/cm<sup>3</sup>, when the data discussed by Clark (25) are used. The zero-pressure high-temperature density for the outer core has been estimated to be  $6.4 \pm 0.5$  g/cm<sup>3</sup> (1) and  $7.2 \pm 0.3$  g/cm<sup>3</sup> (22). These estimates, based on Adams-Williamson solutions for the core, were made on the assumption that the entire outer core is homogeneous. Recent seismic solutions for the core make this assumption questionable. The failure of attempts to fit, simultaneously, the density and compressional velocity of the whole outer core by finite strain theory suggests that this region, even though it is molten, is not homogeneous. The estimates of zero-pressure properties are therefore open to some question.

Fortunately, shock-wave data exist for some iron-nickel and iron-silicon alloys at core pressures, and thus we do not have to rely exclusively on the above extrapolations. There is some uncertainty in the temperature corrections, but these errors are probably much less than the errors involved in extrapolating core properties to standard conditions. McQueen and Marsh (26), on the basis of shock-wave experiments on iron-nickel alloys, concluded that pure iron is about 8 percent denser than the outer core. Knopoff and MacDonald (27) and Birch (23) had previously concluded that the outer core is roughly 15 percent less dense than iron at the same temperature and pressure. In a later paper, Birch (17) reduced this discrepancy to 10 percent. Most of these authors have ignored the roughly 5 percent decrease in density upon melting or have assumed implicitly that shocked metals behave as their melts do.

The bulk sound speed  $C_0$  of the core at zero pressure and high temperature has been estimated to lie between 4.88 and 5.18 km/sec (1, 22). The corresponding values for shocked iron-nickel alloys range from 3.1 to 3.7 km/sec. The decrease in  $C_0$  upon melting is roughly 7 to 15 percent. The shock-wave values should probably be further decreased by a small amount in order to make them comparable to extrapolated core temperature values.

The above results suggest that a pure iron-nickel core has too large a density and too small a bulk sound speed to be compatible with geophysical data. A lighter alloying element that would increase the bulk sound speed is required.

There are two major candidates for

this element. One is silicon (27, 28); the other is sulfur (29). Both elements would have the desired properties of decreasing the density and increasing the seismic velocity of pure iron, as is shown below.

Ringwood (28) has discussed at great length the geochemical arguments for silicon in the core. He argues for a hot origin of the earth and assumes that most of the sulfur escaped from the earth as volatiles. The possibility of sulfur in the core has been discussed extensively by Murthy and Hall (29). They point out that the conditions under which sulfur and silicon go into the core are radically different. The presence of silicon in the core requires large-scale high-temperature reduction and the formation of a massive carbon monoxide atmosphere, which would be blown off after accretion and would carry with it other volatiles (28). On the other hand, even a relatively cold planet (~1000°C) can produce an iron-sulfur core. In the present earth these temperatures are available below about 30 kilometers.

Murthy and Hall (29) compared the relative abundances of such volatile elements as the halogens, rare gases, sulfur, and water in the crust and mantle with chondritic abundances. Sulfur was shown to be depleted in the crust and mantle by several orders of magnitude relative to the other volatile elements. They concluded, on several geochemical grounds, that sulfur was more likely to be incorporated into the earth than not, and, since it was obviously deficient in the crust and upper mantle, it had probably been segregated into the core as a sulfur-rich iron melt. They did not investigate the geophysical implications of their proposal.

Table 4 summarizes the major element compositions of three classes of meteorites and various models for the earth's mantle. No single class of meteorites has the proper overall composition to match the data for the earth. For example, the mean atomic weight of the earth is about 27.0. Meteorites have the following mean atomic weights: carbonaceous chondrites (H<sub>2</sub>O free), 23.4 to 24.0; ordinary chondrites, 24.4; "high iron" chondrites, 25.1; enstatite chondrites, 25.6; and iron meteorites, 55. The earth's core comprises 32.5 percent of the earth's mass as compared with the FeS + Fe + Ni percentages of carbonaceous and ordinary chondrites of 24.0 and 19.2 percent, respectively. By mixing of 40 percent

Table 4. Composition of meteorites, earth, and moon (in percent by weight). The iron meteorites (column 3) are coarse octahedrites. The composition of the mix (column 4) is 40 percent type I carbonaceous chondrites, 46 percent ordinary chondrites, and 14 percent iron meteorites. The composition for "mantle" for this mixture can be well approximated by mixing 75 percent "lower mantle" material with 25 percent "upper mantle" (pyrolite) material. These percentages suggest that the lower mantle begins near a depth of 600 kilometers. For the mix (column 4),  $\langle M \rangle$  (core) = 50.5;  $\rho_0$  (core) = 6.34. For the reduced carbonaceous chondrites I (column 5),  $\langle M \rangle$  (core) = 50.4;  $\rho_0$  (core) = 6.24. Data for the lunar mantle (column 6) are from Urey (46).

Component	Carbonaceous chondrite I	Ordinary chondrite	Iron meteorite	Mix	Reduced carbonaceous chondrite I	Lower mantle	Lunar mantle	Upper mantle
	1	2	3	4	5	6	7	8
SiO <sub>2</sub>	32.5	38.8		49.6	47.7	51	49.1	49.6
MgO	21.9	24.3		32.0	42.0	28	33.8	41.1
FeO	14.5	12.1		18.4	10.3	21	17.1	9.3
Total	68.9	75.2		100.0	100.0	100	100.0	100.0
FeS	23.8	6.0	3.7	12.8				
Fe	0.2	11.8	89.1	18.0	25.9			
Ni	0.0	1.4	7.2	1.7	1.7			
Si					3.5			
Total	24.0	19.2	100.0	32.5	31.1			

carbonaceous I, 46 percent ordinary, and 14 percent iron meteorites, we can obtain the proper core-mantle ratio. These proportions are close to the proportions assumed by Murthy and Hall (29). The mean atomic weight and the zero-pressure density of the resulting core are 50.5 and 6.34 g/cm<sup>3</sup>, respectively; the sulfur content is 14 percent by weight. The density will be reduced by up to 5 percent upon melting. The mantle, for this mix, contains 18.4 percent by weight of FeO. There is good agreement between the mantle composition derived here and that determined in a previous section, as can be seen by comparing columns 4 and 6 in Table 4. Note also the good agreement with Urey's estimate of the composition of the lunar interior (Table 4, column 7). Note the large increase in FeO content of the mantle over that of pyrolite (Table 4, column 8), which is presumably representative of the upper mantle (28).

The "mantle" of the meteorite mix (Table 4, column 4) is more iron rich than solutions for the upper mantle (Table 4, column 8) and slightly less iron rich than solutions for the lower mantle (Table 4, column 6). If we assume that the upper 600 kilometers of the mantle has the composition of pyrolite and that the rest of the mantle has the composition determined for the lower mantle, then the average composition of the mantle is similar to the meteorite mix (Table 4, column 4). Whitcomb and Anderson (7) have previously concluded, on the basis of seismic-wave reflection amplitudes, that the 600-kilometer discontinuity prob-

ably involves a larger density contrast, or is sharper, than the other transition zones in the mantle. Either alternative is consistent with a compositional change, as well as a phase change, being involved at the 600-kilometer discontinuity.

The presence of a light crust and a dense core indicates that the earth is a gravitationally differentiated body. It is usually assumed, however, that the great bulk of the earth—the mantle—is chemically homogeneous. The results presented here suggest that the mantle itself may be gravitationally stratified and that pyrolite may be a differentiate of a more primitive material, just as basalt is a differentiate of pyrolite.

The composition given in column 5 of Table 4 was determined by reducing some of the FeO and SiO<sub>2</sub> of a C-, S-, and H<sub>2</sub>O-free type I carbonaceous chondrite in order to obtain a mantle composition consistent with pyrolite and to obtain the proper silicate metal or mantle-core ratio (28). The resulting core has 11 percent silicon by weight, a mean atomic weight of 50.4, and a zero-pressure density of 6.24 g/cm<sup>3</sup>; the last two values are very close to those estimated above for the iron-sulfur core.

Balchan and Cowan (30) determined the density of shocked iron-silicon alloys at conditions comparable to those in the core and concluded that their results were consistent with a core containing 14 to 20 percent silicon in iron by weight. The zero-pressure, room-temperature densities of these compositions are 7.02 to 7.25 g/cm<sup>3</sup>. The density of  $\alpha$ -iron (7.87 g/cm<sup>3</sup>) is

also much greater than the sulfides of iron; compare, for instance, FeS (troilite), 4.83 g/cm<sup>3</sup>; FeS (sphalerite structure), 3.60 g/cm<sup>3</sup>; FeS (wurtzite structure), 3.54 g/cm<sup>3</sup>; FeS<sub>2</sub> (pyrite), 5.02 g/cm<sup>3</sup>; and FeS<sub>2</sub> (marcasite), 4.89 g/cm<sup>3</sup>.

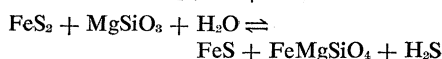
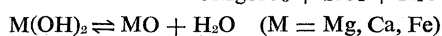
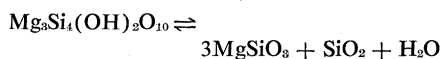
The zero-pressure bulk sound speed,  $C_0$ , of the iron-silicon alloys lies between  $4.1 \pm 0.1$  (4 percent silicon) and  $5.4 \pm 0.1$  km/sec (20 percent silicon). These values bracket estimates for the core. Comparable shock-wave data on the iron sulfides are not available, but zero-pressure ultrasonic data on pyrite (FeS<sub>2</sub>) give a value of 5.23 km/sec (31, 32), which is much higher than the shock-wave speed of 3.45 km/sec for pure iron at zero pressure (26). The bulk sound speeds in such sulfides as CdS and ZnS are 40 to 45 percent greater than in the metal. The approximate zero-pressure bulk sound speed of the FeS-Fe core in Table 4 is 3.9 km/sec. For Ringwood's FeSi core the corresponding value is about 4.2 km/sec. Thus it appears that both silicon and sulfur serve to decrease the density and increase the velocity of iron. These estimates are very crude and do not take into account phase changes or melting. The point is that the two core models have very similar physical properties ( $\langle M \rangle$ ,  $\rho_0$ , and  $C_0$ ). Shock-wave data on Fe-FeS mixtures may be able to resolve the possibilities.

### Origin of the Mantle and Core

Larimer (32) has outlined the condensation history of a cooling gas of cosmic composition. Compounds such as CaTiO<sub>3</sub>, MgAl<sub>2</sub>O<sub>4</sub>, Al<sub>2</sub>SiO<sub>5</sub>, and CaAl<sub>2</sub>Si<sub>2</sub>O<sub>8</sub> will condense first at temperatures between 1740° and 1620°K. Iron will condense next at 1620°K. Magnesium-rich pyroxenes and olivines condense between 1470° and 1420°K; FeS condenses at 680°K, and H<sub>2</sub>O at 210°K. All the above temperatures were calculated on the assumption of a total pressure of  $6.6 \times 10^{-3}$  atmosphere. Larimer and Anders (33) conclude that the fractionation patterns in meteorites occurred in the solar nebula as it cooled from high temperatures and could not be produced in the meteorite parent bodies. Especially, they infer the following accretion temperatures from the abundance patterns: carbonaceous chondrites,  $\leq 400^\circ\text{K}$ ; enstatite and ordinary chondrites,  $400^\circ$  to  $650^\circ\text{K}$ ; and the major fraction of iron meteorites,  $\cong 1100^\circ\text{K}$ .

Accretion of the planets presumably involved planetesimals that condensed over the entire temperature range, although the different planets may have incorporated different proportions of the various condensates. As a planet grows, the accretional energy increases and the temperature at the surface of the body is controlled by a balance between the available gravitational or kinetic energy, the heat capacity and thermal conductivity of the surface layer, the heats of reaction involved in chemical reactions occurring at the surface, and the reradiation of energy to the dust-gas cloud. As the planet grows, it will be less and less capable of retaining the volatiles brought in by the accreting particles, and the fractionation, in time, will be roughly the reverse of the condensation procedure. When the surface temperature reaches 680°K, the reaction  $\text{FeS} + \text{H}_2 \rightarrow \text{Fe} + \text{H}_2\text{S}$  will occur if the planet is accreting in a  $\text{H}_2$ -rich environment; the planet will, thereafter, not be able to incorporate much FeS into its interior. With the previously discussed meteorite mix model for the earth, this temperature was reached when the planet had assembled some 50 percent of its present mass. This would require that the time scale for accretion be much longer than the  $10^5$  to  $10^6$  years discussed by Hanks and Anderson (34). Alternatively, the  $\text{FeS} \cdot \text{H}_2$  reaction could start earlier in the accretional history of the planet if it were not 100 percent efficient, or it would not occur at all if the  $\text{H}_2$  had already left the environment (28).

Reactions such as



between the atmosphere and the surface of the accreting planet could tend to buffer the surface temperature and keep it below 500°K for long periods of time during the accretion process. Substantial amounts of heat could also be buried in the planet by the impacting bodies and be unavailable for reradiation if the rate of accretion is faster than the rate of heat conduction to the surface. The above considerations would prolong the period available for trapping FeS in the interior.

Implicit in the above discussion is the assumption that the planets did not start to accrete until the condensation

process was complete and the solar nebula was relatively cold. A growing planet would incorporate the solid portion of available material—that is, the “local cosmic abundances”—in its interior in its initial stages of growth but could retain only the more refractory compounds as it grew. A large-scale redistribution of material must occur later in its history in order to form a core and to transport the retained volatiles and the less refractory compounds from the center of the body to the surface to form the crust and atmosphere. Thus the earth, for example, must have turned itself inside out to obtain its present configuration.

If the planets accreted while condensation was taking place, a chemically zoned planet would result, with compounds that condense above 1620°K, such as  $\text{CaTiO}_3$ ,  $\text{MgAl}_2\text{O}_4$ ,  $\text{Al}_2\text{SiO}_5$ ,  $\text{CaAl}_2\text{Si}_2\text{O}_8$ , and Fe, forming the central part of the body. In the next 160°K range of cooling, compounds such as  $\text{Ca}_2\text{SiO}_4$ ,  $\text{CaSiO}_3$ ,  $\text{CaMgSi}_2\text{O}_6$ ,  $\text{KAlSi}_3\text{O}_8$ ,  $\text{MgSiO}_3$ ,  $\text{SiO}_2$ , and Ni would condense. Between 1420° and 1120°K the rest of the important mantle minerals,  $\text{Mg}_2\text{SiO}_4$ ,  $\text{NaAlSi}_3\text{O}_8$ , and  $(\text{Na,K})_2\text{SiO}_3$  would condense. Further cooling would bring in such metals as Cu, Ge, Au, Ga, Sn, Ag, Pb, the sulfides of Zn, Fe, and Cd, and, finally,  $\text{Fe}_3\text{O}_4$  (400°K), the hydrated silicates (~300°K),  $\text{H}_2\text{O}$  (210°K), and the rare gases. Turekian and Clark (35) have discussed some of the implications of this model of planetary formation. The scarcity of sulfur, particularly relative to water, in the crust and upper mantle is a major problem since neither the core nor volatility can be invoked, nor can it be argued that carbonaceous chondrites are enriched relative to solar abundances.

#### Formation of an Iron-Sulfur Core

In both of the above models of accretion the composition of the planet changes as it grows, and there is no compelling reason to assume that the composition of the various planets should be the same or the same as any single class of meteorites. The work of Larimer (32) and of Larimer and Anders (33) suggests that carbonaceous chondrites simply represent the last material to condense from a cooling nebula instead of representing primordial material. In the cold accretion model, this material would be mixed with material that condensed at higher

temperatures, such as ordinary chondritic and iron meteorites, to form the nucleus of the accreting planet, which would contain most of the volatiles such as  $\text{H}_2\text{O}$  and FeS. As the planet grows, the material that can be retained on the surface and incorporated into the interior becomes progressively less representative of the material available. In the terminal stages of accretion, the surface temperatures will decrease with time (34) and eventually will be controlled by solar heating.

The amount of volatiles and low-temperature minerals retained by a planet will depend on the fraction of the planet that accretes during the initial and terminal stages. In the accretion-during-condensation model the full complement of volatiles and sulfides must be brought in during the terminal stage. In both of these models much of the material that forms the core (Fe + FeS in the cold accretion model and Fe in the condensation model) is already near the center of the earth. In alternate proposals the core-forming material is either distributed evenly throughout the mantle (23) or at the surface of the accreting planet (28).

One important boundary condition for the formation of the earth is that the outer core, now and probably  $3 \times 10^9$  years ago, be molten. If we take the temperature in the mantle to be 1880°C at 620-kilometer depth (36) and assume an adiabatic temperature gradient of 0.5°C per kilometer from that depth to the core-mantle boundary, the temperature at the top of the core will be about 3000°C, which is of the order of the melting temperature of iron at core pressures. For the condensation model the temperature of the primitive iron core is 1150° to 1350°C and will increase to 2300° to 2500°C, owing to adiabatic compression, when the planet assumes its present size. These temperatures can be compared with Kennedy's (37) estimate of 3725°C for the melting temperature of pure iron at the boundary of the inner core. These temperatures are all subject to great uncertainty, but it appears difficult with the condensation model to have a molten iron core. It is even more difficult to raise the central part of the earth above the melting temperature of pure iron in the cold accretion model (34). It appears that the extra component in the core must also serve to decrease its melting temperature. This is easily accomplished with sulfur.

The eutectic temperature for the sys-

tem Fe-FeS is 990°C and is remarkably insensitive to pressure up to at least 30 kilobars (38). The eutectic composition is 31 percent by weight of sulfur at 1 atmosphere and 27 percent by weight of sulfur at 30 kilobars. In an earth of meteoritic composition a sulfur-rich iron liquid would be the first melt to be formed. Core formation could proceed under these conditions at a temperature some 600°C lower than would be required to initiate melting in pure iron. In the vicinity of the core the eutectic temperature is some 1600°C lower than pure iron. If the earth accreted from cold particles under conditions of radiative equilibrium, the temperatures will be highest in the upper mantle, which is where melting will commence. In most plausible thermal history calculations, the melting point of iron increases with depth much more rapidly than the actual temperatures, and any sinking molten iron will refreeze. Unless the earth was very hot during most of the accretional process, it will be difficult to get the iron to the center of the planet. This difficulty does not occur for the iron-sulfur model of the core, since gravitational accretion energy, adiabatic compression, and radioactive heating bring the temperatures throughout most of the earth above 1000°C early in its history and, probably, during most of the accretional process (34). Since the eutectic temperature seems to be relatively independent of pressure, core formation will be self-sustaining. The increase of gravitational energy due to core formation leads to a temperature rise of about 1600° to 2000°C throughout the earth (34, 39). Such temperatures would be adequate to melt the rest of the iron in the mantle, which would drain into the core, and to cause extensive melting of silicates and differentiation of the crust and upper mantle. The short time scale of accretion required by Hanks and Anderson (34) to form a molten iron core within the first 10<sup>9</sup> years of earth history is no longer required but, of course, cannot be ruled out.

### Possible Core of Mars

The ease of manufacturing a core in the earth might suggest that Mars should have a substantial core. Current estimates of the initial temperature for

Mars, on the assumption of cold accretion, allow it to retain all infalling FeS. The average temperature in Mars below some 600 kilometers is about 1500°C if the planet accreted in  $3 \times 10^5$  years (34), which is well above the Fe-FeS eutectic temperature. The liquidus for an FeS-rich FeS-Fe system is 1100°C at atmospheric pressure, 1600°C at 60 kilobars, and about 3400°C at the center of Mars if the slope of the melting curve of FeS (40) remains constant to hundreds of kilobars. Thus, most of the deep interior of Mars is much closer to the eutectic temperature than to the liquidus temperature, and only a fraction of the planet's complement of Fe and FeS will be molten. For a carbonaceous chondrite I composition, the total FeS plus Fe content is 24 percent by weight. Binder (41) estimated that the mass of a martian core would be 2.7 to 4.9 percent of the mass of the planet, or about 11 to 20 percent of the metallic and sulfide content available. With this model the core of Mars would be richer in sulfur than the core of the earth, and much FeS would be left in the mantle of Mars. The small size of the martian core and the small size of the planet suppress the importance of gravitational heating due to core formation. Actually, the size of the martian core can be considerably greater than that estimated by Binder (41), since he used a zero-pressure density of 8 g/cm<sup>3</sup> for the core. This value is greater than the uncompressed density of the earth's core. If the density of the martian core is bracketed by the density of the earth's core and by the density of the eutectic mix in the system Fe-FeS at 30 kilobars, then the core can be 9 to 15 percent, by mass, of the planet. A satisfactory model for Mars can be obtained by melting most of the FeS and some of the Fe in ordinary chondrites.

### References and Notes

1. F. Birch, *J. Geophys. Res.* **57**, 227 (1952).
2. O. L. Anderson, E. Schreiber, R. C. Liebermann, N. Soga, *Rev. Geophys.* **6**, 491 (1968).
3. L. R. Johnson, *J. Geophys. Res.* **72**, 6309 (1967); *Bull. Seismol. Soc. Amer.* **59**, 973 (1969); D. L. Anderson and B. R. Julian, *J. Geophys. Res.* **74**, 3281 (1969); D. L. Anderson and T. Jordan, in preparation.
4. A. L. Hales and J. L. Roberts, in preparation; D. Helmlinger and R. A. Wiggins, in preparation.
5. D. L. Anderson, *Special Paper No. 3*, B. A. Morgan, Ed. (Mineralogical Society of America, Washington, D.C., 1970), pp. 85-93.
6. — and C. Sammis, *Phys. Earth Planet. Interiors* **3**, 41 (1970).

7. J. H. Whitcomb and D. L. Anderson, *J. Geophys. Res.* **75**, 5713 (1970).
8. J. B. Walsh, *ibid.* **74**, 4333 (1969).
9. V. D. Esheby, *Proc. Roy. Soc. Ser. A* **241**, 376 (1957).
10. F. Birch, in *The Earth's Crust and Upper Mantle*, P. J. Hart, Ed. (American Geophysical Union, Washington, D.C., 1970).
11. H. Spetzler and D. L. Anderson, *J. Geophys. Res.* **73**, 6051 (1968).
12. F. Birch, *Bull. Seismol. Soc. Amer.* **29**, 463 (1939).
13. C. G. Sammis, D. L. Anderson, T. Jordan, *J. Geophys. Res.* **75**, 4478 (1970).
14. D. S. Hughes and J. L. Kelly, *Phys. Rev.* **92**, 1145 (1953); R. A. Toupin and B. Bernstein, *J. Acoust. Soc. Amer.* **33**, 216 (1961).
15. O. L. Anderson and R. C. Liebermann, *Phys. Earth Planet. Interiors* **3**, 61 (1970).
16. C. G. Sammis, *Geophys. J. Roy. Astron. Soc.* **19**, 285 (1970).
17. F. Birch, *J. Geophys. Res.* **69**, 4377 (1964).
18. D. L. Anderson and T. Jordan, *Phys. Earth Planet. Interiors* **3**, 23 (1970). The abbreviation F<sub>90</sub> represents 90 (mole) percent forsterite (Mg<sub>2</sub>SiO<sub>4</sub>), 10 percent fayalite (Fe<sub>2</sub>SiO<sub>4</sub>).
19. S. P. Clark, Jr., and A. E. Ringwood, *Rev. Geophys.* **2**, 35 (1964).
20. L. Thomsen, *J. Chem. Phys. Solids*, in press.
21. D. L. Anderson, *Geophys. J. Roy. Astron. Soc.* **13**, 9 (1967); *J. Geophys. Res.* **74**, 3857 (1969).
22. R. G. McQueen, S. P. Marsh, J. N. Fritz, *J. Geophys. Res.* **69**, 2047 (1964); D. L. Anderson and H. Kanamori, *ibid.* **73**, 6477 (1968); T. J. Ahrens, D. L. Anderson, A. E. Ringwood, *Rev. Geophys.* **7**, 667 (1969).
23. F. Birch, *Geophys. J. Roy. Astron. Soc.* **4**, 295 (1961).
24. D. L. Anderson, *Earth Planet. Sci. Lett.* **5**, 89 (1968).
25. S. P. Clark, Jr., in *The Earth Sciences: Problems and Progress in Current Research*, T. W. Donnelly, Ed. (Univ. of Chicago Press, Chicago, 1963), pp. 5-42.
26. R. G. McQueen and S. P. Marsh, *J. Geophys. Res.* **71**, 1751 (1966).
27. L. Knopoff and G. J. F. MacDonald, *Geophys. J. Roy. Astron. Soc.* **3**, 68 (1960).
28. A. E. Ringwood, in *Advances in Earth Science*, P. M. Hurlley, Ed. (M.I.T. Press, Cambridge, Mass., 1966), pp. 287-356.
29. V. R. Murthy and H. T. Hall, *Phys. Earth Planet. Interiors* **2**, 276 (1970).
30. A. S. Balchan and G. R. Cowman, *J. Geophys. Res.* **71**, 3577 (1966).
31. G. Simmons, *J. Grad. Res. Cent.* **34**, 1 (1965).
32. J. W. Larimer, *Geochim. Cosmochim. Acta* **31**, 1215 (1967).
33. — and E. Anders, *ibid.*, p. 1239.
34. T. Hanks and D. L. Anderson, *Phys. Earth Planet. Interiors* **2**, 19 (1969).
35. K. Turekian and S. P. Clark, Jr., *Earth Planet. Sci. Lett.* **6**, 346 (1969).
36. D. L. Anderson, *Science* **157**, 1165 (1967).
37. G. C. Kennedy, *Phys. Rev. Lett.* **16**, 608 (1966).
38. R. Brett and P. M. Bell, *Earth Planet. Sci. Lett.* **6**, 479 (1969).
39. F. Birch, *J. Geophys. Res.* **70**, 6217 (1965).
40. W. E. Sharp, *ibid.* **74**, 1645 (1969).
41. A. B. Binder, *ibid.*, p. 3110.
42. A. E. Ringwood, *Phys. Earth Planet. Interiors* **3**, 109 (1970).
43. M. Kumazawa and O. L. Anderson, *J. Geophys. Res.* **74**, 5961 (1969).
44. R. C. Liebermann, thesis, Columbia University (1969).
45. M. Manghani, *J. Geophys. Res.* **74**, 4317 (1969).
46. H. C. Urey, personal communication.
47. D. L. Anderson and M. Smith, *Trans. Amer. Geophys. Union* **49**, 282 (1968).
48. H. Mizutani, Y. Hamano, Y. Ida, S. Akimoto, *J. Geophys. Res.* **75**, 2741 (1970).
49. Supported by NSF grant GA-12703 and NASA grant NGL-05-002-069. We thank R. Murthy and H. T. Hall for a preprint of their paper. This article is adapted from an address delivered 16 April 1970 in Cambridge, Massachusetts, at a symposium in honor of Professor Francis Birch. A complete account will appear in the proceedings volume [*The Nature of the Solid Earth*, E. C. Robertson, Ed. (McGraw-Hill, New York, in press)]. Contribution 1903, Division of Geological Sciences, California Institute of Technology.